

# Irradiation-free, columnar defects comprised of self-assembled nanodots and nanorods resulting in strongly enhanced flux-pinning in $\text{YBa}_2\text{Cu}_3\text{O}_{7-\delta}$ films

A Goyal<sup>1,3</sup>, S Kang<sup>1</sup>, K J Leonard<sup>1</sup>, P M Martin<sup>1</sup>, A A Gapud<sup>1</sup>,  
M Varela<sup>1</sup>, M Paranthaman<sup>1</sup>, A O Ijaduola<sup>2</sup>, E D Specht<sup>1</sup>,  
J R Thompson<sup>1,2</sup>, D K Christen<sup>1</sup>, S J Pennycook<sup>1</sup> and F A List<sup>1</sup>

<sup>1</sup> Oak Ridge National Laboratory, Oak Ridge, TN 37831, USA

<sup>2</sup> University of Tennessee, Knoxville, TN 37996-1200, USA

E-mail: [goyala@ornl.gov](mailto:goyala@ornl.gov)

Received 21 September 2005, in final form 3 October 2005

Published 11 October 2005

Online at [stacks.iop.org/SUST/18/1533](http://stacks.iop.org/SUST/18/1533)

## Abstract

The development of biaxially textured, second-generation, high-temperature superconducting (HTS) wires is expected to enable most large-scale applications of HTS materials, in particular electric-power applications. For many potential applications, high critical currents in applied magnetic fields are required. It is well known that columnar defects generated by irradiating high-temperature superconducting materials with heavy ions significantly enhance the in-field critical current density. Hence, for over a decade scientists world-wide have sought means to produce such columnar defects in HTS materials without the expense and complexity of ionizing radiation. Using a simple and practically scalable technique, we have succeeded in producing long, nearly continuous vortex pins along the *c*-axis in  $\text{YBa}_2\text{Cu}_3\text{O}_{7-\delta}$  (YBCO), in the form of self-assembled stacks of  $\text{BaZrO}_3$  (BZO) nanodots and nanorods. The nanodots and nanorods have a diameter of  $\sim 2\text{--}3$  nm and an areal density ('matching field') of 8–10 T for 2 vol.% incorporation of  $\text{BaZrO}_3$ . In addition, four misfit dislocations around each nanodot or nanorod are aligned and act as extended columnar defects. YBCO films with such defects exhibit significantly enhanced pinning with less sensitivity to magnetic fields *H*. In particular, at intermediate field values, the current density,  $J_c$ , varies as  $J_c \sim H^{-\alpha}$ , with  $\alpha \sim 0.3$  rather than the usual values 0.5–0.65. Similar results were also obtained for  $\text{CaZrO}_3$  (CZO) and YSZ incorporation in the form of nanodots and nanorods within YBCO, indicating the broad applicability of the developed process. The process could also be used to incorporate self-assembled nanodots and nanorods within matrices of other materials for different applications, such as magnetic materials.

<sup>3</sup> Address for correspondence: Metals and Ceramics Division, Oak Ridge National Laboratory, PO Box 2008, MS 6116, Oak Ridge, TN 37831-6116, USA.

## 1. Introduction

Second-generation HTS conductors or ‘coated conductors’ comprise a flexible metallic substrate upon which several buffer layers and then the superconducting layer are deposited [1]. The key goal is to have a biaxially textured superconducting layer so that few high-angle, weakly conducting grain boundaries are present. This is accomplished by epitaxial formation of the superconducting layer on biaxially textured oxide surfaces deposited upon the flexible metallic substrate. Three techniques have been developed to accomplish this—ion-beam assisted deposition (IBAD) [5] of biaxially textured buffers on polycrystalline alloy substrates, epitaxial deposition of buffer multilayers on rolling assisted, biaxially textured substrates (RABiTS) [6], and inclined substrate deposition (ISD) [7] of buffers on polycrystalline alloy substrates. For epitaxial YBCO on substrates fabricated using all three techniques, the ‘*inter-granular*’ critical current density is enhanced due to suppression of weak links at grain boundaries. However, for practical application of HTS materials, the in-field performance or the *intra-granular* critical current density also needs to be enhanced further. The first significant progress towards this goal was made by incorporation of randomly distributed BaZrO<sub>3</sub> (BZO) nanoparticles of size 5–100 nm with a modal particle size of 10 nm [8]. It was shown that the incorporation of randomly distributed, heteroepitaxial BZO particles introduces significant strain in the YBCO lattice due to the large lattice mismatch between BZO and YBCO. This was shown to generate misfit dislocations aligned along the crystallographic *c*-direction of YBCO, with an areal density of 400  $\mu\text{m}^{-2}$  compared to 80  $\mu\text{m}^{-2}$  for an undoped YBCO film. These defects resulted in a 1.5–2-fold improvement in the in-field  $J_c$  in the magnetic field range 1–5 T. Another recent report, describing depositions of multi-layers of Y<sub>2</sub>BaCuO<sub>5</sub> (211) and YBCO, demonstrated that nanoparticles can once again be incorporated into the YBCO film [9]. In this case, the nanoparticles of average size  $\sim$ 15 nm are aligned along the *ab*-planes (i.e., parallel to the Cu–O sheets of the layered superconductor), with an areal density of  $\sim$ 1.1  $\times$  10<sup>11</sup> particles  $\text{cm}^{-2}$ . It was found that both the self-field and in-field  $J_c$  were enhanced by the incorporation of such particles. Here we use a simple and industrially scalable route to produce columnar defects that are self-assembled stacks of nanodots and nanorods of non-superconducting phases within epitaxially grown YBCO films on RABiTS substrates to achieve massive enhancements of the in-field  $J_c$ .

## 2. Experimental details

Self-assembled nanodots and nanorods of non-superconducting phases were incorporated by performing laser ablation from a single target comprising a mixture of YBCO powder and nanoparticles of the chosen non-superconducting phase. Nanoparticles of materials such as BZO, CaZrO<sub>3</sub> (CZO), YSZ, Ba<sub>*x*</sub>Sr<sub>1–*x*</sub>TiO<sub>3</sub> (BST) etc are commercially available from vendors such as Sigma-Aldrich. These nanoparticles, with a sharp particle size distribution ranging from 10 to 100 nm, are well mixed with YBCO powder. The resulting composite powder is then pressed and sintered to form a target for pulsed laser deposition (PLD). All depositions were performed on the

technically important RABiTS substrates with the configuration Ni–5 at.% W (50  $\mu\text{m}$ )/Y<sub>2</sub>O<sub>3</sub> (75 nm)/YSZ (75 nm)/CeO<sub>2</sub> (75 nm) [10]. PLD depositions were performed using a XeCl (308 nm) excimer laser, LPX 305 at a repetition rate of 10 Hz, substrate deposition temperature of 790 °C and an oxygen partial pressure of 120 mTorr. The transport critical current density ( $J_c$ ) was measured using the standard four-point probe method using a voltage criterion of 1  $\mu\text{V cm}^{-1}$ .

## 3. Results and discussion

Figure 1 shows cross-section transmission electron microscopy (TEM) images of the YBCO film. Figure 1(a) shows columns of BZO nanodots aligned along the [001] or the crystallographic *c*-axis of YBCO. The red arrows on the image point to the various columns of BZO. The image was taken with the sample tilted along the  $g = 001$  vector of the YBCO film in order to better visualize the columnar properties of the nanoparticles due to their relatively small size compared to the local thickness of the TEM sample. Figure 1(b), taken from a different region in the sample, indicates that nanorods of BZO are also present. The relative fraction of BZO incorporated as nanodots and nanorods as determined by TEM observations is about 60% nanodots and 40% nanorods. Figure 2(a) shows a plan view TEM image in low magnification, directed down the crystallographic *c*-axis of YBCO. The image shows the areal distribution of nanodots and nanorods within the thin section of a TEM foil. The intersecting lines within the particles are extinction bands, with the left side of the image being a thicker region of the TEM foil than that of the right. From the areal density of BZO nanoparticles in figure 2(a), one finds a matching field, a magnetic field with equivalent vortex density  $B_\phi = \phi_0/a^2$ , of  $\sim$ 8–10 T, where  $\phi_0 = 2.07 \times 10^{-11}$  T  $\text{cm}^2$  is the flux quantum and  $a$  is the average in-plane separation of vortices. Figure 2(b) is a higher magnification image, clearly showing that the contrast seen in figures 1 and 2(a) is from distinct particles of a different phase. The array of BZO nanodots and/or nanorods can be approximated by a square lattice with a lattice spacing,  $a \sim$  15 nm, as evident from figure 2(b). Figure 2(c) shows a Z-contrast STEM image of a single nanodot within the YBCO matrix. Around each BZO nanodot, misfit dislocations can be seen. Since the nanodots and nanorods are aligned along the *c*-direction of YBCO, the strain from the misfit dislocations is also aligned and extended. For this unique configuration, these BZO nanodots and nanorods and the correlated misfit dislocations around them may be expected to form ideal flux-pinning sites similar to damage tracks by heavy-ion irradiation [2–4].

The superconducting transport properties of epitaxial YBCO films, 0.2  $\mu\text{m}$  thick, fabricated both with and without incorporation of self-assembled nanodots and nanorods are shown in figure 3. Figure 3(a), a plot of transport  $J_c$  versus applied field,  $H$ , for YBCO and YBCO + 2 vol.% BZO sample with  $H \parallel c$  at 77 K, shows that the dopants reduce the sensitivity to magnetic field. For example, at an applied field of 1.5 T,  $J_c$  for the sample with BZO nanodots and nanorods decreases only by a factor of five compared to a factor of  $\sim$ 12 for undoped YBCO. The enhancement in  $J_c$  can be seen for all fields despite a decrease in the transition temperature of the doped film ( $\sim$ 87 K as determined magnetically via a SQUID

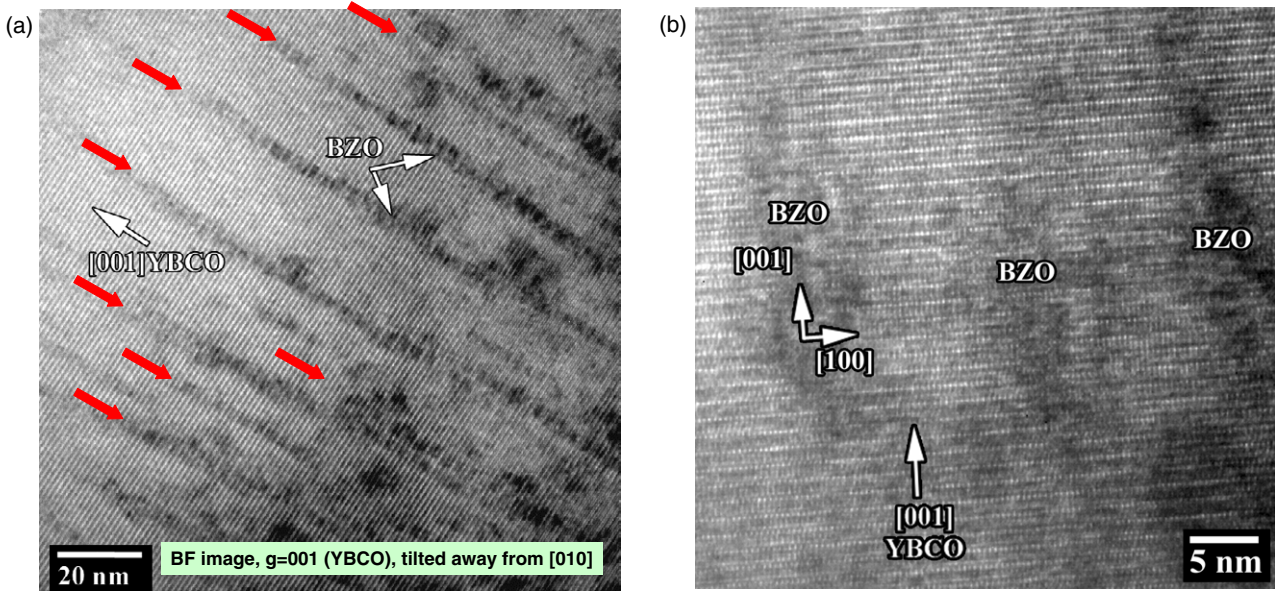


**Figure 1.** Cross-section transmission electron micrograph (TEM) of a YBCO film on RABiTS with self-assembled nanodots and nanorods of  $\text{BaZrO}_3$  (BZO). (a) Image shows that BZO nanodots are aligned along the crystallographic  $c$ -direction in YBCO and are about 2–3 nm in diameter. (b) Cross-section image showing the presence of nanorods in addition to nanodots.

magnetometer) compared to the undoped film ( $T_c \sim 90$  K). Figure 3(b) shows a log–log plot of  $J_c$  normalized to self-field  $J_c$  versus applied field. It can be seen that the exponent in the power-law relationship  $J_c \sim H^{-\alpha}$  is 0.31 for the film containing the BZO nanodots and nanorods, compared to 0.5 for the undoped YBCO film. This reduced fall-off in  $J_c$  as a function of applied field shows the strong pinning for  $H \parallel c$  for the doped samples. Figure 3(c) shows the angular dependence of  $J_c$ , taken at 77 K and 1 T applied field. The angular dependence curve is shifted to higher  $J_c$  at all angles. In particular, a very pronounced peak for  $H \parallel c$  (angle =  $0^\circ$ ) can be observed, indicative of strong pinning defects along the  $c$ -axis for the film containing BZO nanodots and nanorods. In order to obtain higher-field and lower-temperature data, a 2 mm wide bridge was patterned on the samples (the original width of the sample was 5 mm) to meet the maximum measuring current restrictions in the system used for these measurements. During the patterning process and subsequent handling, some sample degradation does occur and the self-field  $J_c$  is reduced slightly. Nevertheless, the data shown in figure 3(d) of transport  $J_c$  versus  $H$  at higher applied fields applied parallel to the  $c$ -axis at 77, 65 and 40 K adequately show the trends and improvement in  $J_c$  obtained. The data show that the enhancement of  $J_c$  at higher fields (over 7 T) with self-assembled BZO nanodots and nanorods is even more significant, a factor of six or more; this improvement in  $J_c$  also extends to lower temperatures, as is evident in figure 3(d).

It is not meaningful to compare the magnitude of the transport  $J_c$  shown in figure 3 to the data reported in [8] since the films here are thinner and  $J_c$  generally depends on thickness, typically decreasing exponentially with increase in thickness [11, 12]. However, comparison with the method suggested in [9], i.e. multilayering of a YBCO film with 211/123 layers to form rows of 211 nanoparticles perpendicular

to the  $c$ -axis, is possible, since films of similar thickness have been grown on RABiTS substrates [13, 14]. The angular dependence of  $J_c$  at 77 K, 1 T, is markedly different for films on RABiTS using the 211/123 multilayering approach compared to the approach reported in this paper. It is found that while the peak at  $H \parallel ab$  is similar in both samples, the 211/123 multilayered sample has no  $J_c$  peak for  $H \parallel c$ . Hence, significantly superior pinning is observed over a broad angular range for the present case of self-assembled BZO nanodot and nanorod incorporation. Compared to YBCO films without the incorporation of self-assembled nanodots and nanorods, the data in figure 3(a) show a factor of  $\sim 5$  improvement in  $J_c$  in the field range 0.4–1.5 T at 77 K, and over a factor of six beyond 7 T. This improvement is better than what was reported for incorporation of randomly distributed nanoparticles of BZO in the range of 5–100 nm [8]. Driscoll *et al* [8] show that incorporation of randomly distributed BZO nanoparticles within epitaxial YBCO films on single-crystal and IBAD substrates results in an enhancement of  $J_c$  by a factor of 1.5–2 over a field range of 1–5 T and a factor of five above 7 T.

Detailed x-ray analysis and selected area electron diffraction in TEM show that the BZO nanodots and nanorods are epitaxial with the YBCO matrix. Since BZO and YBCO have about a 9% lattice mismatch, significant strain is expected during the growth of the film. It is speculated that minimization of this large misfit strain is the driving force for the vertical self-assembly of BZO nanodots and nanorods within the YBCO film. The question now arises of whether this simple method can be extended to incorporation of other materials into YBCO films. Figure 4(a) shows cross-section TEM images for incorporation of 2 vol.%  $\text{CaZrO}_3$  (CZO) nanodots and nanorods within the YBCO film using the same technique as described above. Figure 4(b) is a cross-section TEM image for

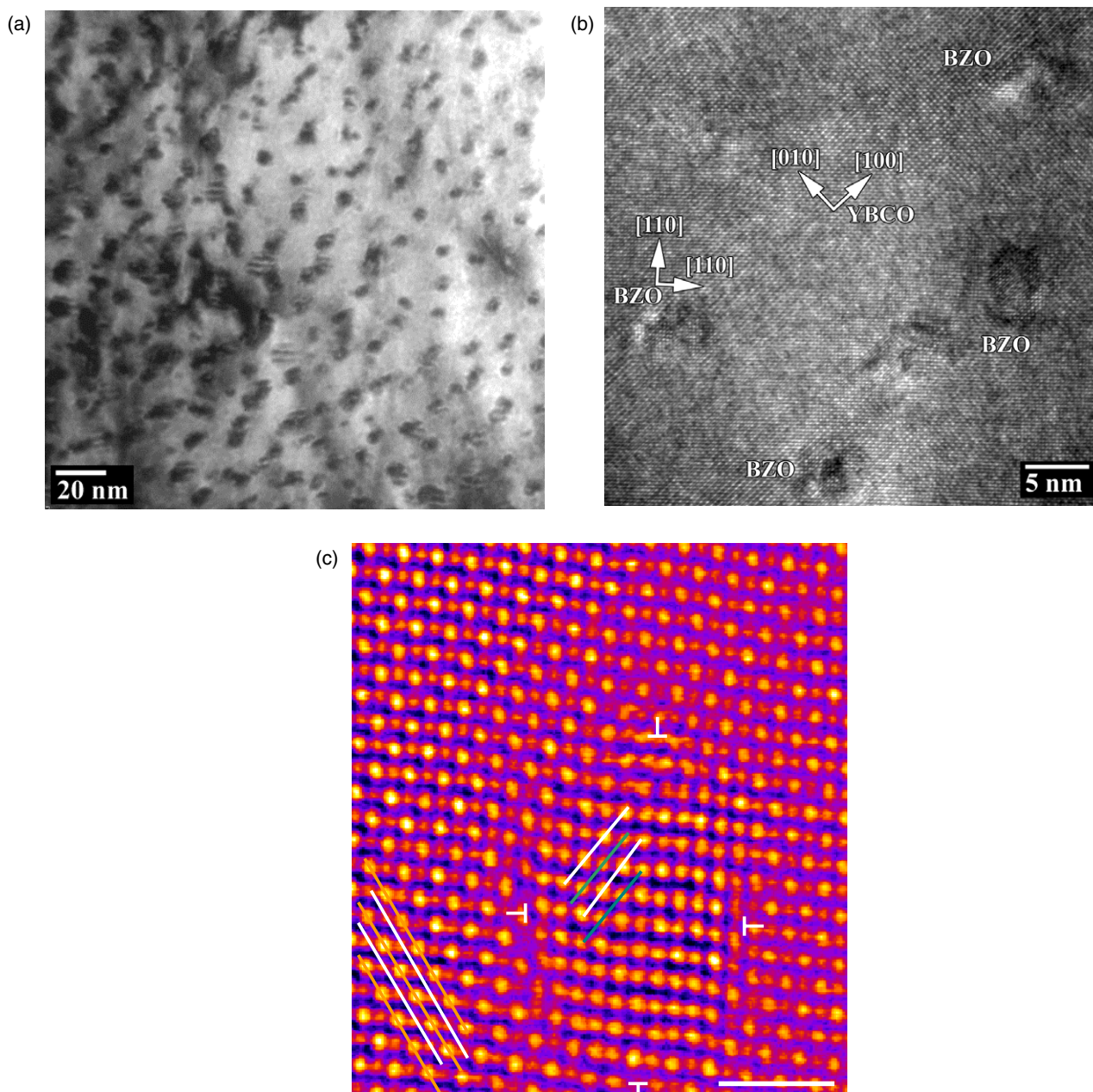


**Figure 2.** Plan-view TEM images of the YBCO film on RABiTS with self-assembled nanodots and nanorods of  $\text{BaZrO}_3$  (BZO). (a) Low-magnification image showing the high density of nanodots and nanorods. (b) Higher-magnification image showing that the BZO nanodots and nanorods within the YBCO are about 2–3 nm in diameter and can be approximated as situated on a square lattice with a spacing of  $\sim 15$  nm. (c) Z-contrast STEM image of a single BZO nanodot. The extra semiplane in the edge dislocation cores is marked in white. Four misfit dislocations can be seen around the BZO nanodot. Since the BZO nanodots are aligned along the  $c$ -direction, the strain is also aligned, forming an extended defect. In the YBCO, the BaO planes have been marked with white lines, while CuO lines are marked with yellow lines. In the BZO nanoparticle, the ZrO planes have been marked with green lines, and the BaO planes again with white lines. The scale bar is 1.5 nm.

incorporation of 1 vol.% YSZ nanodots and nanorods within the YBCO film using the same method. The YBCO film in figure 4(b) was tilted off its [010] axis to better visualize the formation of nanorods through the effects of the electron beam interactions through the TEM foil. For the case of CZO, more self-assembled nanodots are seen; for YSZ, more nanorods are seen compared to BZO. The differences in relative volume fractions of nanodots and nanorods are expected to relate to

differences in lattice misfit strain as well as reactions of the inclusions with YBCO. For example, in the case of YSZ, the self-assembled nanodots and nanorods have reacted with YBCO to form BZO. The angular dependence of  $J_c$  at 77 K, 1 T shows significant enhancement over undoped YBCO even though the transition temperatures are significantly reduced for these films, to  $T_c = 85$  K for the 1 vol.% YSZ and to 80 K for the 2 vol.% CZO doped film. Overall, the TEM images and

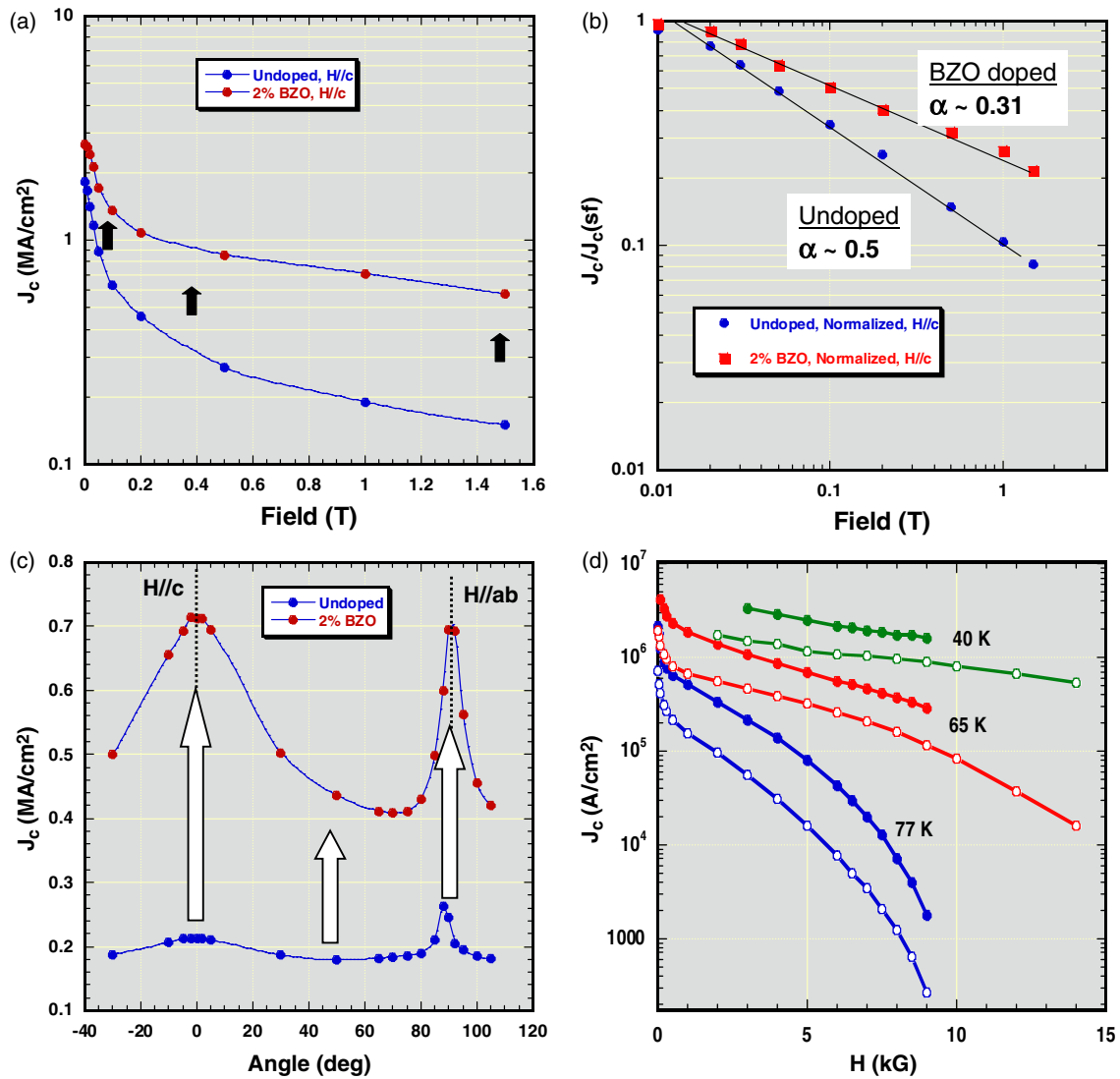


**Figure 3.** Superconducting transport properties of YBCO films on RABiTS. (a) Critical current density,  $J_c$ , as a function of applied magnetic field for an undoped YBCO film on RABiTS compared to a YBCO film with 2 vol.% incorporation of BZO nanodots and nanorods. A very significant enhancement of  $J_c$  is seen for all fields. (b) Log–log plot of normalized  $J_c$  as a function of applied field, showing that the power-law exponent in the relation,  $J_c \sim H^{-\alpha}$ , is only 0.31 for the YBCO film with self-assembled nanodots and nanorods, compared to 0.5 for the undoped film. (c) Angular dependence of  $J_c$  at 77 K, 1 T for an undoped YBCO film on RABiTS compared to a YBCO film with 2 vol.% incorporation of BZO nanodots and nanorods. Measurements were made in a configuration such that the applied field is always perpendicular to the current. As can be seen, massive enhancement of  $J_c$  is observed at all angles, in particular for  $H \parallel c$  (angle =  $0^\circ$ ). (d)  $J_c$  versus applied magnetic field,  $H$ , for high fields as a function of measurement temperature for an undoped YBCO film on RABiTS, compared to a YBCO film with 2 vol.% incorporation of BZO nanodots and nanorods. Large increases in  $J_c$  can be seen for all fields at all measurement temperatures.

the observation of angular peaks in  $J_c$  for  $H \parallel c$ -axis show that this method can produce correlated nanostructures with a variety of dopant materials.

Since the first public disclosure of the work reported in this paper in several conferences last year and early this year [15–18], significant interest in this work has generated world-wide attention. Delay in the publishing of these results has stemmed from the time required for a patent application to be filed [19]. A good confirmation of the results reported here is the very recent work of Yamada *et al* [20], which has reproduced the same microstructure of columnar, self-aligned nanodots following the method reported here [15–19]. Yamada *et al* show incorporation of columnar defects of BZO nanodots

in 0.25  $\mu\text{m}$  thick  $\text{GdBa}_2\text{Cu}_3\text{O}_{7-x}$  and  $\text{SmBa}_2\text{Cu}_3\text{O}_{7-x}$  films on IBAD substrates via PLD. For reasons which are unclear, in their work no improvement in  $J_c$  is found for fields up to 2 T for  $\text{GdBa}_2\text{Cu}_3\text{O}_{7-x}$  films and up to 6 T for the  $\text{SmBa}_2\text{Cu}_3\text{O}_{7-x}$  films. At higher fields, where improvement in  $J_c$  is observed, the relative effects are smaller than those reported here.

It should be possible to use a similar approach to incorporate nanodots and nanorods of one phase into another for other applications, particularly for ceramic inclusions within a ceramic matrix. Composites of metal/alloy nanodots within a ceramic matrix should also be possible. Significant interest has been shown recently for potential uses of such composites for applications other than superconductivity [21–23].

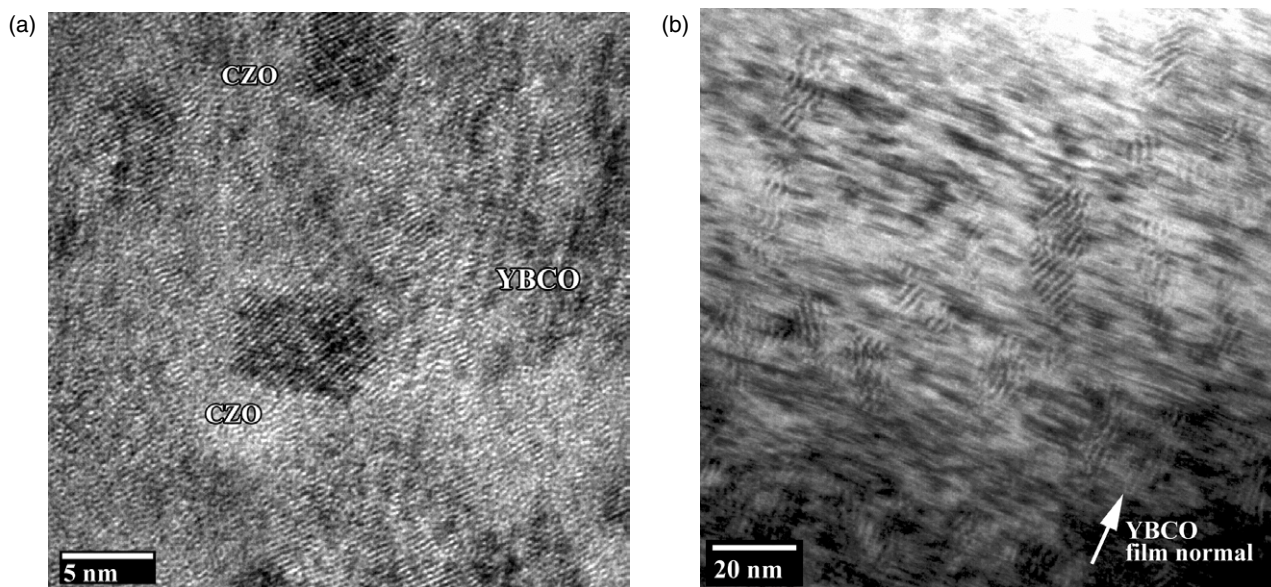


**Figure 4.** Cross-section TEM images for YBCO films on RABiTS: (a) film with 2 vol.%  $\text{CaZrO}_3$  (CZO) nanodots and nanorods; (b) YBCO film with 1 vol.% YSZ nanorods.

## Acknowledgments

Research sponsored by the US Department of Energy, Office of Electricity and Delivery Reliability—Superconductivity Program, under contract DE-AC05-00OR22725 with UT-Battelle, LLC, managing contractor for Oak Ridge National Laboratory. The authors would also like to thank the American Superconductor Corporation for providing the high-quality RABiTS substrates used for this work.

## References

- [1] Goyal A (ed) 2004 *Second Generation HTS Conductors* (Boston, MA: Kluwer Academic) (ISBN 1-4020-8117-0)
- [2] Civale L *et al* 1991 *Phys. Rev. Lett.* **67** 648–51
- [3] Weinstein R *et al* 2005 *Supercond. Sci. Technol.* **18** S188–93
- [4] Li Q *et al* 2005 *IEEE Trans. Appl. Supercond.* **15** 2787–9
- [5] Groves J R *et al* 2002 *Physica C* **382** 43–7
- [6] Goyal A *et al* 1996 *Appl. Phys. Lett.* **69** 1795–7
- [7] Bauer M, Semerad R and Kinder H 1999 *IEEE Trans. Appl. Supercond.* **9** 1502
- [8] Macmanus-Driscoll J L *et al* 2004 *Nat. Mater.* **3** 439–43
- [9] Haugan T *et al* 2004 *Nature* **430** 867–9
- [10] Goyal A, Schoop U and Paranthaman P 2004 *MRS Bull.* **29** 552–63
- [11] Foltyn SR *et al* 1999 *Appl. Phys. Lett.* **75** 3692
- [12] Kang BW *et al* 2002 *J. Mater. Res.* **17** 1750
- [13] Haugan T *et al* 2005 *Physica C* **425** 21–6
- [14] Gapud A *et al* 2005 *Appl. Phys. Lett.* to be submitted
- [15] Goyal A *et al* 2004 Presented at the 2004 Annual Peer Review of the US Superconductivity Program for Electric Systems (July 2004) Full viewgraphs of the presentations made at this meeting were available within one month of the meeting at the website: [http://www.energetics.com/meetings/supercon04/pdfs/presentations/f\\_rabits\\_strategic\\_talk\\_ffy04\\_final.pdf](http://www.energetics.com/meetings/supercon04/pdfs/presentations/f_rabits_strategic_talk_ffy04_final.pdf)
- [16] Goyal A *et al* 2004 CCA 2004: Presented at the Int. Workshop on Coated Conductor for Applications (Oiso Prince Hotel, Kanagawa, Japan, Nov. 2004)
- [17] Gapud A *et al* 2005 Presented at the 2005 Wire Development Workshop (St. Petersburg, FL, Jan. 2005) Full viewgraphs of the presentations made at this meeting were available a few weeks after the meeting at the website: <http://www.energetics.com/meetings/wire05/pdfs/session3/session3c.pdf>
- [18] Kang S *et al* 2005 Presented at the MRS Spring Meeting (San Francisco, CA, April 2005)
- [19] UT-Battelle/ORNL 2005 US Patent Application Filed
- [20] Yamada Y *et al* 2005 *Appl. Phys. Lett.* **87** 132502
- [21] Narayan J and Tiwari A 2004 *J. Nanosci. Technol.* **4** 726–32
- [22] Tiwari A *et al* 2003 *J. Nanosci. Technol.* **3** 368–71
- [23] Kumar D *et al* 2002 *J. Mater. Res.* **17** 738–42